Modification of the DD Neutron Emission Spectrum at the 2.4 - 2.5 MeV Energy Range in Neutral-Beam-Injection-Heated Plasma and Its Application to Fuel Ion Ratio Diagnostics

Tomoki URAKAWA and Hideaki MATSUURA

Department of Applied Quantum Physics and Nuclear Engineering, Kyushu University, 744 Motooka, Fukuoka 819-0395, Japan

(Received 17 June 2020 / Accepted 13 September 2020)

In neutral-beam-injection (NBI)-heated plasma, the emission spectra of the neutrons produced by D(d,n)^{3}He and T(d,n)α fusion reactions are known to be distorted from Gaussian distribution functions in both the high and low energy sides along the NBI direction. This study shows that the effect of NBI heating can be applied to the central energy region, i.e., the 2.4 - 2.5 MeV range in the D(d,n)^{3}He neutron emission spectrum. Conventionally, the intense spectrum anisotropy appears via the anisotropy in the double-differential D(d,n)^{3}He cross-section. Herein, we have shown the anisotropy in the neutron emission spectrum of the central energy range (2.4 - 2.5 MeV) due to the alteration of the neutron emission spectrum (2.4 - 2.5 MeV). Caused by the modification of the deuteron velocity distribution function is large enough to negate the anisotropy caused by the double-differential D(d,n)^{3}He cross-section. An application of the anisotropy effect to fuel-ion ratio diagnostics is discussed, and the attendant degree of improvement is evaluated.

Keywords: double differential neutron emission spectrum, anisotropic neutron emission, fuel ion ratio diagnostic

DOI: 10.1585/pfr.15.1403080

1. Introduction

In a burning plasma, fast ions are generated via fusion reactions and external heating, and an energetic non-Maxwellian component is formed in the ion-velocity distribution functions [1–6]. A rise in the fast-ion population induces a distortion of the emission spectra of fusion-produced particles from a Gaussian distribution [7] and enhances the D(d,n)^{3}He fusion reaction rate coefficient, leading to an increase in the total emission rate. As an example of this, Fig. 1 indicates the neutron emission spectrum distortion. The solid line displays the emission spectrum distorted from the Gaussian distribution. The split line indicates the Gaussian distribution. The emission spectra distortion has been employed as a yardstick for investigating fast-ion diagnostics aimed at understanding the energetic ion characteristics in core plasma [8–11]. Herein, an α particle "knock-on" process was observed via the measurements of the deuterium-tritium (DT) neutron emission spectra distortion [8, 9]. The fast-ion distributions that emerged following an experiment involving third harmonic ICRF heating on deuterium beams using neutron emission spectrometry were also examined [10]. Furthermore, a novel method was proposed for determining the fuel-ion ratio by measuring the distorted DT neutron emission spectra [11].

In neutral-beam-injection (NBI)-heated plasma, a non-Maxwellian component formed in the velocity distribution function exhibits anisotropy in a particular direction due to external beam injection. The emission spectrum generated through a fusion reaction is anisotropically distorted due to the velocity distribution function with an anisotropic non-Maxwellian component [from Gaussian distribution to the higher (lower) energy side toward (opposite to) the NBI direction]. It has been comprehensively analyzed using double-differential emission spectra [12]. In this study, the double-differential emission spectrum ex-

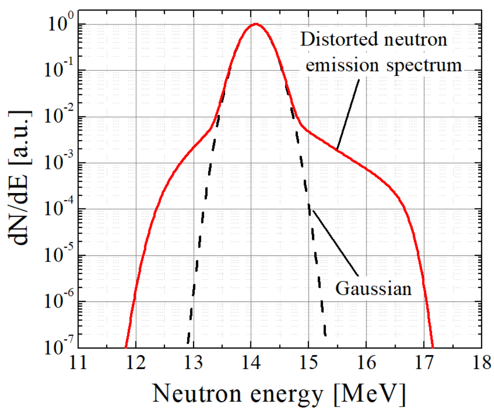

Fig. 1 Emission spectra of neutron produced by T(d,n)α reaction. Solid line shows distorted emission spectrum due to fusion reaction of fast ions. Dashed line shows Gaussian.

author's e-mail: urakawa-0804@nucl.kyushu-u.ac.jp

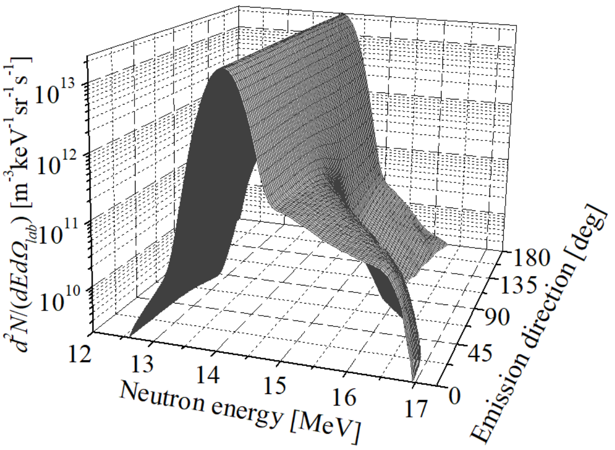

Fig. 2 Double differential emission spectra of neutron produced by T(d,n)α reaction as a function of energy and emission angle. The emission angle is defined the angle between the direction of the emitted neutron and that of the beam injection in the laboratory system.

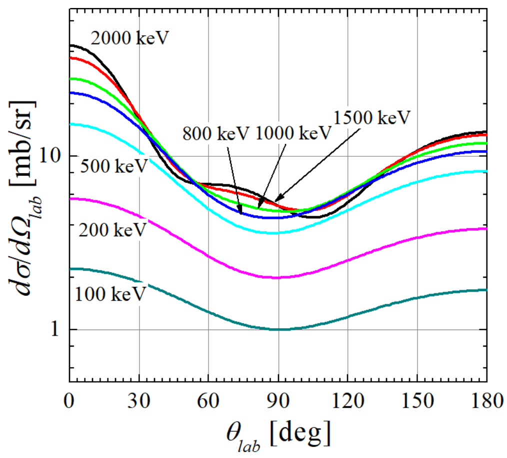

Fig. 3 Differential cross section of D(d,n)^{3}He fusion reaction.

plains the emission rate of the particles emitted per unit energy, unit solid angle in the laboratory system, and unit volume (as shown in Fig. 2). The anisotropy is also caused by the differential cross-section of the D(d,n)^{3}He reaction (Fig. 3) [13]. As the beam energy increases, the neutrons produced by the D(d,n)^{3}He reaction tend to be emitted in a forward direction toward the NBI. The neutron emission rate measured at the neutron flux monitor near the equatorial port was reported to be greater than that measured above the LHD central axis in large helical device (LHD)-based deuterium plasma experiments using tangential NBI [14, 15].

To date, numerous studies on the large distortion of the high-energy side along the NBI direction and its practical applications have been carried out [16, 17]. However, the effect on the neutron emission spectrum at the central energy region (2.4 - 2.5 MeV for deuterium–deuterium (DD) neutrons and 13.5 - 15 MeV for DT neutron) has not yet been comprehensively discussed. Just as the distortion toward both high (above 2.7 MeV for DD neutrons) and low (below 2.2 MeV for DD neutrons) energy sides are due to the NBI heating, the central energy region of the emission spectrum is also modified, such as anisotropy along with the increase in emission rate. Modification in this region can lead to an improvement in the diagnostic performance, thus, studying the properties and the plasma-parameter dependency is important.

A method for measuring the central energy region of neutron spectra involves fuel ion diagnostics using neutron measurements [18–22]. From the measurement of the intensity of each neutron, the fuel ion ratio, n_t/n_d, is given as follows [18]:

$$n_t/n_d = \frac{R_{DT} < \sigma v >_{DD}}{2R_{DD} < \sigma v >_{DT}}, \tag{1}$$

where n_t and n_d are the triton and deuteron number densities, respectively. $R_{DT(DD)}$ is the DT (DD) reaction rate and $<\sigma v>_{DT(DD)}$ is the DT (DD) reaction rate coefficient. A serious issue of this diagnostics is that the detection of DD neutron (signal) is interfered with by the slowing-down component of DT neutrons in the form of noise. In the case of thermal plasma, the detectable parameter range has been reported as $n_t/n_d < 0.6$ and $T_i > 6$ keV [19]. To improve the measurement performance, a technique using the increase in the fraction of the DD to DT reaction rate during NBI heating was proposed [19, 22]. However, this technique has not been examined in terms of the various plasma parameters [19, 22]. Besides, the neutron emission spectra were assumed to be isotropic.

In this study, we evaluated the modification at the central energy region (2.4 - 2.5 MeV for DD neutrons) of the neutron emission spectrum due to NBI heating. It was assumed that the neutrons were produced by the D(d,n)^{3}He reaction in NBI-heated DT plasma (e.g., international thermonuclear experimental reactor (ITER)-like plasma). The enhancement of the measurement performance of fuel-ion ratio diagnostics using anisotropic neutron emission spectra was also discussed as an example of the implementation of this specific modification. Section 2 describes the method of calculation and the model for transporting neutrons. Results and discussion are shown in Sec. 3. Finally, the concluding remarks are given in Sec. 4.

2. Calculation Methods

2.1 Double differential neutron emission spectrum

2.1.1 2-dimensional ion velocity distribution function in NBI-heated plasma

Figure 4 shows the velocity distribution function of the beam-injected deuteron. With the assumption of the NBI-heated DT plasma (approximately 300 MW, electron density $n_e = 7.0\times10^{19}$ m^{-3}, electron temperature $T_e = 10$ keV, beam power $P_{NBI} = 33$ MW, beam energy $E_{NBI} = 1.0$ MeV, and plasma volume $V_p = 800\,\mathrm{m}^3$), a fast-deuteron slowing-down distribution was obtained. This velocity distribution function was calculated using the analytic model written as follows [23]:

$$f_b(v,\mu) = \frac{S^0\tau_s}{v^3+v_c^3}\sum_{l=0}^{\infty}\frac{(2l+1)}{2}P_l(\mu_b)P_l(\mu) \cdot\left[\left(\frac{v^3}{v_b^3}\right)\left(\frac{v_b^3+v_c^3}{v^3+v_c^3}\right)\right]^{\frac{1}{6}l(l+1)Z_2}U(v_b-v), \quad (2)$$

where S^0 is the number of beam particles per unit volume, τ_s is the Spitzer slowing-down time, P_l is the Legendre polynomials, μ_b is the beam incident pitch angle, v_b is the incident beam particle velocity, v_c is the critical velocity at which ions and electrons lose their energies by collisions at equal rates, Z_2 is the effective charge of the background ions, and U is the unit step function. Besides, the velocity distribution function of triton and deuteron (bulk ion components) was indicated to be a Maxwellian distribution. The relationship between the electron (n_e) and ion density (n_i) was assumed to be $n_e = n_t + n_d^{bulk} + n_d^{beam}$, where n_t is triton density, n_d^{bulk} is deuteron (balk component) density, and n_d^{beam} is beam deuteron density.

2.1.2 Calculation of the double-differential neutron emission spectrum

The double-differential neutron emission spectrum was calculated using the method described in Ref. [12], with the spectrum written as follows:

$$\frac{d^2N_n}{dEd\Omega_{lab}}(E,\theta_{lab}) = \frac{1}{1+\delta_{DD(T)}}\iiint f_D(|\vec{v}_D|)f_{D(T)}(|\vec{v}_{D(T)}|)\frac{d\sigma}{d\Omega} \times\delta(E-E_n)\delta(\Omega_{lab}-\Omega_n)v_r d\vec{v}_D d\vec{v}_{D(T)}d\Omega. \quad (3)$$

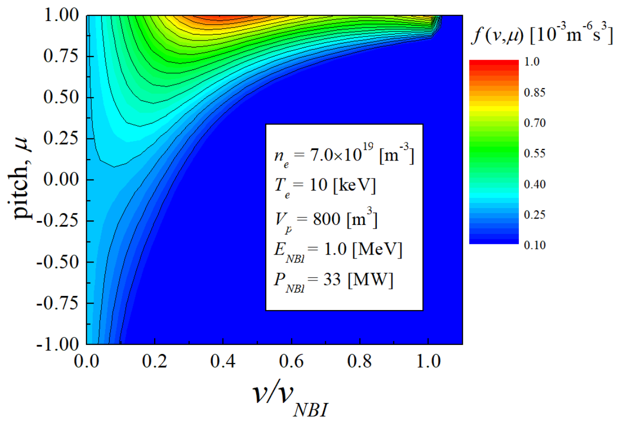

Fig. 4 2D velocity distribution function of beam-injected deuterons. Assuming the ITER like DT plasma, beam-injection energy is 1.0 MeV, and beam power is 33 MW.

Here, E_n is the neutron energy in the laboratory system [24]:

$$E_n = \frac{1}{2}m_nV_c^2 + \frac{m_{^3He(\alpha)}}{m_n+m_{^3He(\alpha)}}(Q_{DD(DT)}+E_r) + V_c\cos\theta_c\sqrt{\frac{2m_{^3He(\alpha)}}{m_n+m_{^3He(\alpha)}}(Q_{DD(DT)}+E_r)}, \quad (4)$$

where θ_{lab} represents the angle between the direction of the emitted neutron and that of the beam injection in the laboratory system, $m_{n(^3He,\alpha)}$ is the neutron (3-helium, α-particle) mass, V_c is the center-of-mass velocity of the colliding particles, θ_c is the angle between the center-of-mass velocity and the neutron velocity in the center-of-mass frame, $Q_{DD(DT)}$ is each reaction's Q-value. Ω_n represents a unit vector in the direction of the neutron emission in the laboratory system, which was determined using classical kinematics as a function of $\vec{v}_D$, $\vec{v}_{D(T)}$, and θ_c. And E_r represents the relative energy given by

$$E_r = \frac{1}{2}\frac{m_Dm_{D(T)}}{m_D+m_{D(T)}}|\vec{v}_D-\vec{v}_{D(T)}|. \quad (5)$$

2.2 Neutron transport calculation

2.2.1 Blanket and collimator model

Figure 5 shows the computational schema of the blanket system with the incorporation of a collimator (detection surface). The blanket model presented a torus form with a major radius of 6.2 m and a minor radius of 2.0 m. The blanket material components and the layer thicknesses are shown in Table 1 [25]. We considered an ITER-like blanket and ensured that the component material of each layer was homogeneous. The detector (collimator) was horizontally installed on the equatorial plane of the torus. The

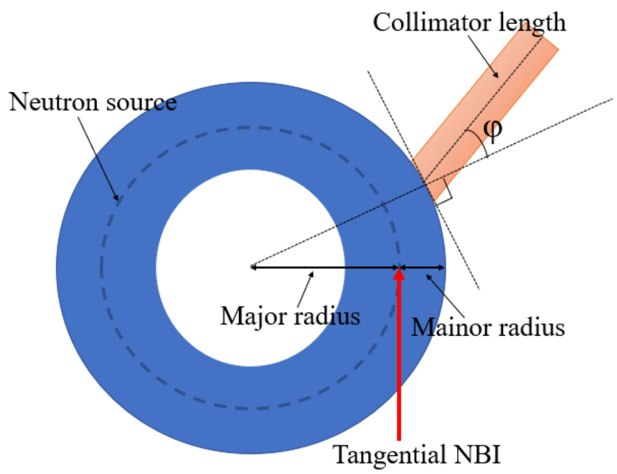

Fig. 5 The model used for MVP neutron transport calculations assuming the ITER condition. The φ shows the angle between the collimator direction and normal from center of torus.

Table 1 Blanket material component.

	Thickness	Component
Be armor	10 mm	Be (100)
Heat sink	22 mm	CuCrZr (82.9), H2O (17.1)
First Wall	49 mm	SS316L(N)-IG (84.6), H2O (15.4)
Gap	3 mm	
Shield structure	370 mm	SS316L(N)-IG (72), H2O (18)

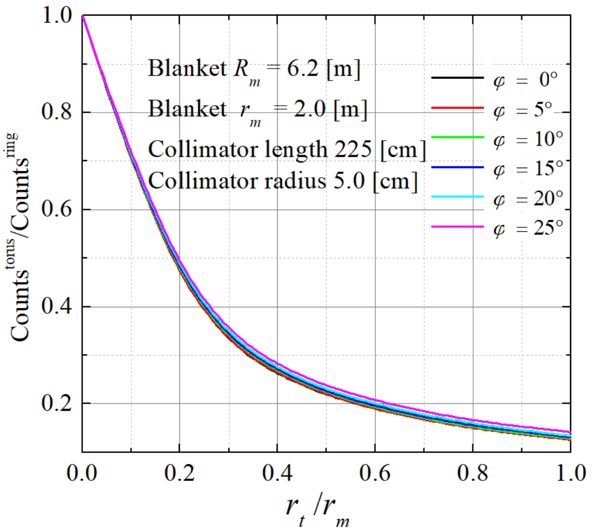

Fig. 6 The count ratio when using the torus volume (uniform emissivity) and ring sources. r_t indicates the minor radius of torus volume source. Count$^{torus(ring)}$ indicates the neutron count number at the detection point when using torus volume (ring) source. Y-axis is ratio to counts using the ring source (r_t/r_m = 0.0).

collimator direction, φ, was set to be the angle created by the radial line from the center of the toroidal surface when viewed from the blanket (upper view), as shown in Fig. 5. The collimator was a pillar type with an inner diameter of 10 cm, an outer diameter of 20 cm, and length of 225 cm. These conditions were set based on Ref. [21].

2.2.2 Calculation of the incident neutron spectrum on the detector

The incident DD neutron spectrum on the detector (signal) and the slowing-down component of the DT neutrons (noise) were calculated using the Monte Carlo transport code MVP [26] with reference to the JENDL-4.0 [27] nuclear data library. The neutron spectra were used as the source in the neutron transport calculations. The incident DD neutron spectra counts on the detector were corrected for geometric detection efficiency based on a torus volume source with uniform emissivity [20]. Figure 6 shows the count ratio when using the torus volume and ring sources. Here, r_t is the minor radius of the torus volume source, and r_m is the plasma minor radius. Count$^{torus(ring)}$ indicates the neutron count number at the detection point when using torus volume (ring) source. In this study, the minor radius of the torus volume was assumed to be 1.2 m (r_t/r_m = 0.6) [20]. We adopted a point detector estimator to calculate the signal and noise. The validity of this calculation method is demonstrated in Ref. [19]. The measurement energy range of neutron detection was set to 2,460 ± 120 keV [19]. The calculation error of each spectrum in the measurement energy region was less than 1.0%.

3. Result and Discussion

3.1 Influence of the modification at the center of the energy region

3.1.1 Double-differential neutron emission spectra

Figure 7(a) shows the double-differential emission spectrum of the neutrons produced by the D(d,n)^{3}He reactions as a function of the neutron emission angle energy and direction. Here θ_{lab} represents the angle between the direction of the emitted neutron and that of the beam injection in the laboratory system. The emission spectra for the neutron emission angles of θ_{lab} = 0°, 90°, and 180° are shown in Fig. 7(b). These spectra were calculated using the velocity distribution function shown in Fig. 4 (T_e = 10 keV, $n_e = 7 \times 10^{19}$ m^{-3}, E_{NBI} = 1.0 MeV, and P_{NBI} = 33 MW). A "ridge" appeared in the central energy region (close to 2.5 MeV), with a peak at around θ_{lab} = 90°. This phenomenon could be attributed to the change of shape of the emission spectrum depending on the emission direction. At θ_{lab} = 0° (180°), the emission spectra were distorted from a Gaussian distribution to the high (low) energy side, with no modification effect was detected in the central energy region. Meanwhile, at θ_{lab} = 90°. The neutron emission energy was approximately 2.5 MeV and the modification appeared around the central energy region, which resulted in a 2.4 - 2.5 MeV emission energy increase in neutron emissions. The emission rate of these neutrons at approximately θ_{lab} = 90° was higher than that at other emission directions (Fig. 7(b)).

Figure 8 shows the neutron emission rate as a function of the emission angle, which was obtained by integrating the spectra over, first, the 2.4 - 2.5 MeV range and, second, the full energy range. The solid lines represent the emission rate when considering an anisotropic D(d,n)^{3}He differential cross-section, while the dashed lines represent the rate when assuming an isotropic D(d,n)^{3}He differential cross-section. The emission rates while considering an isotropic beam injection (emission spectrum) are indicated by the dotted lines on the same planes. From Fig. 8(a), we can see that the 2.4 - 2.5 MeV neutron emission rate was maximized at θ_{lab} = 100°, even though the forward emission was dominated (Fig. 8(b)) by the anisotropy of the D(d,n)^{3}He differential cross-section. An approximate

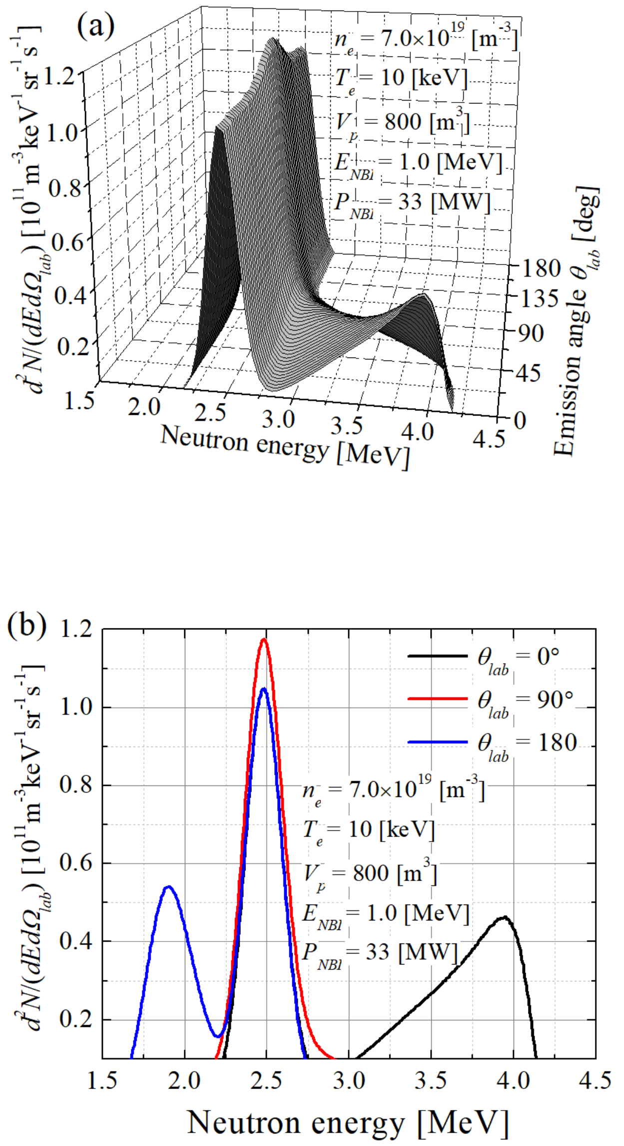

Fig. 7 Double differential neutron emission spectra produced by the D(d,n)^{3}He reactions as a function of neutron energy and emission angle: (a) all emission directions and (b) in directions of θ_{lab} = 0°, 90° and 180°. The θ_{lab}, represents the angle between the direction of emitted neutron and that of beam-injection in the laboratory system. P_{NBI} = 33 MW, E_{NBI} = 1.0 MeV, T_e = 10 keV, and n_e = 7.0 × 10^{19} m^{-3} are assumed.

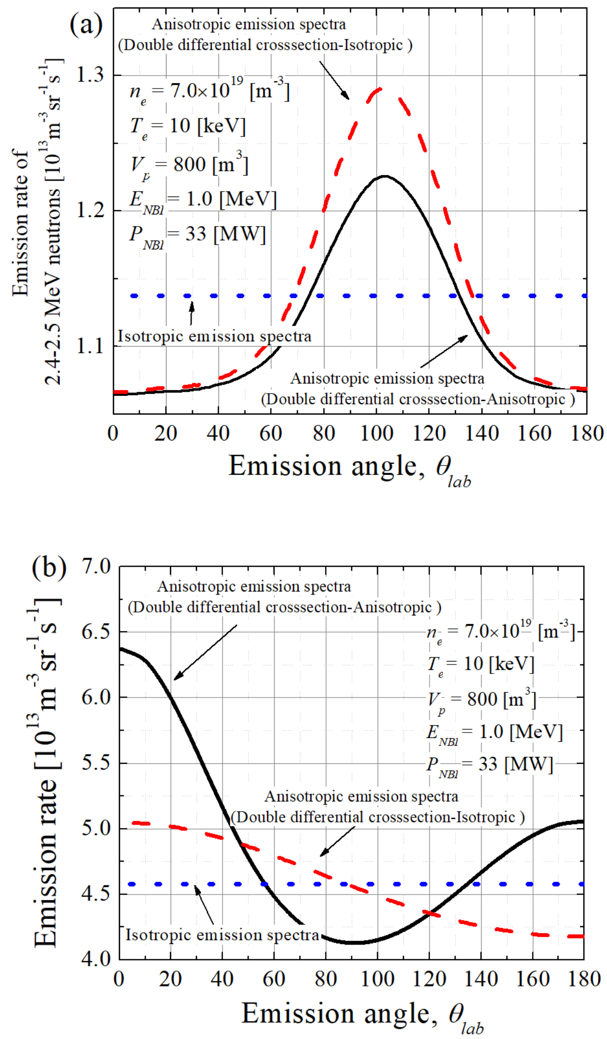

Fig. 8 Emission angle distribution of neutron emission rate obtained by integrating the spectrum of Fig. 5 (Solid line) (a) over 2.4 - 2.5 MeV and (b) over the full range energy. Also shows the emission rate when anisotropic emission spectrum assuming double differential cross section as isotropic (Dashed line) and when isotropic emission spectrum (Dotted lines). P_{NBI} = 33 MW, E_{NBI} = 1.0 MeV, T_e = 10 keV, and n_e = 7.0 × 10^{19} m^{-3} are assumed.

15% (20%) difference in the emission rate of the 2.4 - 2.5 MeV neutrons between θ_{lab} = 100° and 0° can be observed when the anisotropic (isotropic) D(d,n)^{3}He differential cross-section is assumed. Since the intensity of the Gaussian component formed by the D(d,n)^{3}He reaction in thermal plasma is small, the influence of the modification in the central energy region via NBI heating is considerable. Therefore, the increase in the 2.4 - 2.5 MeV neutron emission rate at around θ_{lab} = 100° becomes a significant difference, one that would appear to be direction-dependent. Furthermore, assuming an isotropic D(d,n)^{3}He differential cross-section, the ratio of the forward neutron emission to the total neutron emission decreases, while the ratio of the neutron emission around the vertical direction (θ_{lab} = 90°) increases. Therefore, the difference in the emission rate of the 2.4 - 2.5 MeV neutrons between θ_{lab} = 100° and 0° increases. Herein, the emission rate of neutrons at 2.4 - 2.5 MeV increased by 8% relative to the isotropic emission spectrum at θ_{lab} = 100°.

3.1.2 Effect of electron density, temperature, and neutral-beam-injection power and energy on the central energy region modification

In this section, we examined how the modification of the emission spectrum at the central energy region depends

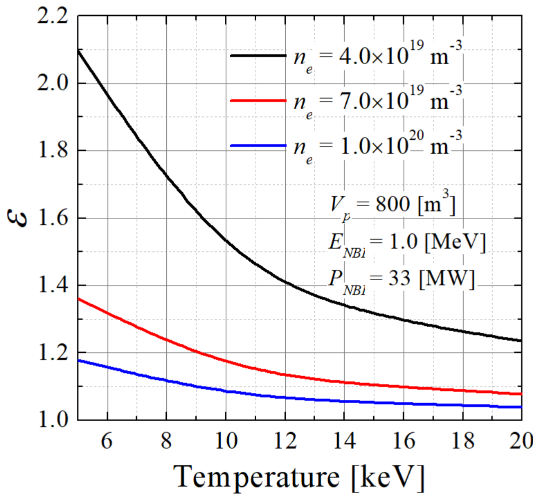

Fig. 9 Density and temperature dependence of the ratio of 2.4 - 2.5 MeV neutrons produced in θ_{lab} = 100° and θ_{lab} = 0°(ε). Assuming the ITER like DT plasma (V_p = 800 m^{-3}), beam-injection energy is 1.0 MeV, and beam power is 33 MW.

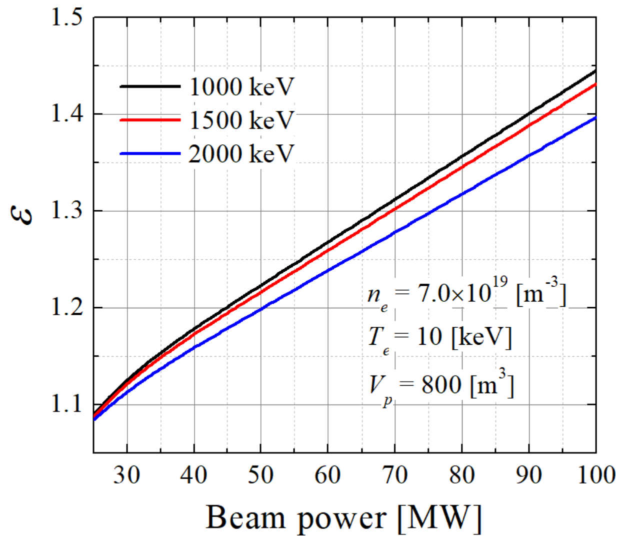

Fig. 10 NBI power and energy dependence of the ratio of 2.4 - 2.5 MeV neutrons produced in θ_{lab} = 100° and θ_{lab} = 0°(ε). NBI power is made with 20 - 100 MW, bean energies with 1.0, 1.5, 2.0 MeV. And assuming the ITER like DT plasma (T_e = 10 keV, $n_e = 7.0 \times 10^{19}$ m^{-3}, V_p = 800 m^{-3}).

on T_e, n_e, E_{NBI}, and P_{NBI}. A parameter ε (ratio of 2.4 - 2.5 MeV neutrons produced at θ = 100° to those produced at θ = 0°) to express the degree of modification:

$$\varepsilon = \frac{\int_{2.4\,MeV}^{2.5\,MeV} \left[\frac{d^2N_n}{dEd\Omega_{lab}}(E,\theta_{lab})\right]_{\theta_{lab}=100^\circ} dE}{\int_{2.4\,MeV}^{2.5\,MeV} \left[\frac{d^2N_n}{dEd\Omega_{lab}}(E,\theta_{lab})\right]_{\theta_{lab}=0^\circ} dE}. \quad (6)$$

Figure 9 shows the ε value as a function of the plasma temperature for various electron densities. For the calculations, an ITER-like DT plasma (E_{NBI} = 1.0 MeV and P_{NBI} = 33 MW) was assumed. When a T_{e} of 5 keV and an n_{e} of 4.0×10^{19} m^{-3} were assumed, the ε value was found to be approximately 2.1; while, when a T_{e} of 20 keV and an n_{e} of 1.0×10^{20} m^{-3} were assumed, the ε value was found to be only 1.05. Thus, the ratio of 2.4 - 2.5 MeV neutrons produced at θ_{lab} = 100° to that produced at θ_{lab} = 0° is remarkably large in low-density and low-temperature regions. In low-density plasma, since the number of incident fast ions is constant, the bulk ion component density decreases. Besides, since the slowing down of the fast ions is mitigated, the ratio of fast-ion density to the total density increases. In addition, the mean energy of the bulk ion component decreases in low-temperature plasma; while the ratio of fast-ion density to total density decreases since a slowing down of the fast ions is promoted. Therefore, as these phenomena decrease the intensity of the Gaussian component produced by the reaction between the bulk ion components, the modification effect in the central energy region increases.

Figure 10 shows the ε value as a function of the NBI power for several beam-injection energies, i.e., E_{NBI} = 1.0, 1.5, and 2.0 MeV for the ITER-like DT plasma (T_{e} = 10 keV, $n_{\mathrm{e}} = 7.0 \times 10^{19}$ m^{-3}, V_{p} = 800 m^{-3}). When E_{NBI} = 1.0 MeV and P_{NBI} = 50 (100) MW, the ε value was evaluated to be 1.23 (1.45). The degree of the modification increased when the fast-ion population was enhanced with the increase in beam power. Meanwhile, when the beam energy increased, the number of incident fast ions decreased, as did the degree of the modification. In the case of E_{NBI} > 1.0 MeV, the effect of the D(d,n)^{3}He cross-section increase was small, while the ratio of the forward emission to total emission increased due to the anisotropic D(d,n)^{3}He double-differential cross-section (Fig. 3).

3.2 Application to fuel ion ratio diagnostic using neutron measurement

In this section, we discuss the improvement in the measurement performance of the fuel-ion ratio diagnostics when using the anisotropic neutron emission spectra. Figure 11 shows the incident neutron emission spectrum at the detector point as a function of the energy and detector installation direction φ, i.e., the angle between the collimator direction and the normal direction from the center of the torus. A collimator length of 225 cm, radius of 5.0 cm, and bin width of 40 keV were assumed. The neutron spectrum was calculated based on the anisotropic spectrum when T_{e} = 10 keV, $n_{\mathrm{e}} = 7.0 \times 10^{19}$ m^{-3}, and $n_{\mathrm{t}}/n_{\mathrm{d}}$ = 1.0. As shown in Fig. 11, the peak count appeared at around $\varphi = -5°$, which was because the angle at which the 2.4 - 2.5 MeV neutron emission rate was the maximum appeared behind the vertical direction (θ_{lab} = 90°) to the direction of the injected beam. With this, the detector direction was fixed at $\varphi = -5°$, and the improvement

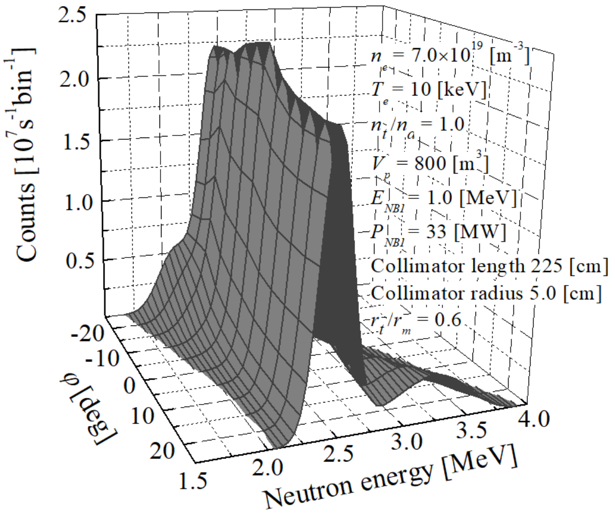

Fig. 11 Double differential incident neutron spectra at the detection point. φ shows the angle between the collimator direction and normal from center of torus. And, the bin-wide is 40 keV: Plasma parameters are P_{NBI} = 33 MW, E_{NBI} = 1.0 MeV, T_e = 10 keV, and $n_e = 7.0 \times 10^{19}$ m^{-3}.

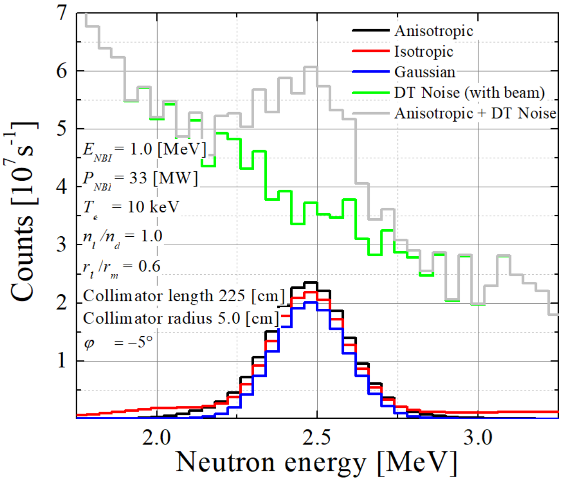

Fig. 12 Neutron spectra at the detection point. Neutron source was calculated based on each spectrum. (Anisotropic, Isotropic and Gaussian); P_{NBI} = 33 MW, E_{NBI} = 1.0 MeV, T_e = 10 keV, and $n_e = 7.0 \times 10^{19}$ m^{-3} are assumed.

in the measurement performance of the fuel-ion ratio diagnostics was evaluated. Figure 12 shows the incident neutron spectra at the detector point for each spectrum (anisotropic, isotropic, and Gaussian) and the slowing-down component of DT neutrons ($\varphi = -5°$). In terms of the anisotropic spectrum, an approximate 5% improvement was observed in the count rate compared to the isotropic emission spectrum. As Fig. 8(a) shows, the emission rate of the 2.4 - 2.5 MeV neutrons increased by 8% compared to the isotropic emission spectrum at $\theta_{lab} = 100°$. The improvement in the count rate reflected this result. Besides,

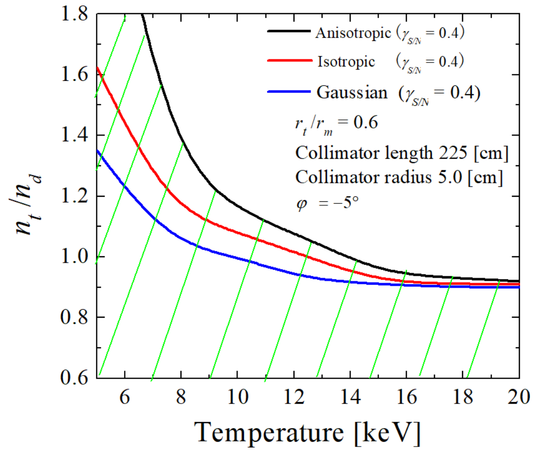

Fig. 13 Contour with $\gamma_{S/N}$ = 0.4 by each spectra measurement as a function of temperature and n_t/n_d. Diagonal lines indicate measurable range ($\gamma_{S/N} > 0.4$) when measuring anisotropic emission spectra.

when compared to the Gaussian spectrum, the anisotropic-related count increased by approximately 15%.

In this study, the S/N value, $\gamma_{S/N}$, is given by

$$\gamma_{S/N} = \frac{\int_{2460-120\,keV}^{2460+120\,keV} \frac{dN^{DD}}{dE}(E)dE}{\int_{2460-120\,keV}^{2460+120\,keV} \frac{dN^{DT}}{dE}(E)dE}, \tag{7}$$

where $dN/dE(E)$ is the incident DD (DT) neutron energy spectrum on the detector. As shown in a previous study [20], the DD neutron and the slowing-down component of the DT neutron can be distinguished when $\gamma_{S/N} > 0.4$. As shown in Fig. 12, the value of $\gamma_{S/N}$ for the anisotropic emission, isotropic emission, and Gaussian spectra were 0.43, 0.41, and 0.38, respectively. Herein, $\gamma_{S/N} > 0.4$ could be achieved using the NBI heating (isotropic or anisotropic spectrum). The contours where $\gamma_{S/N}$ = 0.4 obtained by each spectrum measurement (anisotropic, isotropic, and Gaussian) as a function of temperature and n_t/n_d are shown in Fig. 13. The diagonal lines (green color) in Fig. 13 indicate the measurable region using the anisotropic neutron emission spectrum. Due to the consideration of the anisotropy, the measurement performance was improved, especially in the low-temperature region, which was because, as noted in Sec. 3.1.2, the effect of the modification at the central energy region is significant in low-temperature regions. As a result, while the detectable parameters were n_t/n_d = 1.0 and $T_e \leq$ 12 keV when measuring the isotropic neutron emission spectrum, the range of the detectable parameters was n_t/n_d = 1.0 and $T_e \leq$ 15 keV when measuring the anisotropic neutron emission spectrum. Also, with a low temperature (T_e = 5 keV), it is possible to attain n_t/n_d = 2.0, These results show that considering an anisotropic emission spectrum of neutrons is effective in improving measurement performance of diagnostic fuel-ion ratios.

4. Conclusion

In this study, by assuming an ITER-like NBI-heated DT plasma, the modification at the central energy region of the neutron emission spectra (D(d,n)^{3}He reaction) was evaluated. The modification at the central energy region led to a directional dependence for the emission rate of the neutrons with emission energy of 2.4 - 2.5 MeV, with the maximum emission rate at $\theta_{lab} = 100°$. The degree of the direction dependence increased as the ion temperature and electron density decreased. The difference in the emission rate between $\theta_{lab} = 0°$ and $\theta_{lab} = 100°$ reached 20% (200%) when $T_e = 10$ (5) keV, $n_e = 7.0$ (5.0) $\times 10^{19}$ m^3, $E_{\rm NBI} = 1.0$ MeV, and $P_{\rm NBI} = 33$ MW. Besides, the modification effect in the central energy region was considerable when the NBI power was increased. The difference in emission rate between $\theta_{lab} = 0°$ and 100° reached 25% (50%) when $E_{\rm NBI} = 1.0$ MeV, $P_{\rm NBI} = 50$ (100) MW, $T_e = 10$ keV, and $n_e = 7.0 \times 10^{19}$ m^{-3}.

We also demonstrated that by considering the direction dependence of the emission rate of 2.4 - 2.5 MeV neutrons, the performance of the fuel-ion ratio diagnostic method using neutron measurement can be improved. When the angle between the collimator installation direction and the radiation direction (vertical line) at the center of the torus was 5°, the number of incidents 2.32 - 2.57 MeV neutrons increased by about 5% compared to the isotropic emission. As a result, the S/N value was improved, and S/N > 0.4 was achieved even when $n_t/n_d = 1.0$ and $T_e = 15$ keV. Also, with a low temperature (e.g., $T_{\rm e} = 5$ keV), measuring up to $n_t/n_d = 2.0$ was possible when measuring anisotropic neutron emission spectra.

The effect of modification of the neutron emission spectra in the central energy region is induced by the fast ions in the burning plasma. Thus, measuring neutrons in this region of energy could potentially be applied to rapid-ion diagnosis. Further detailed research is required, however, to better understand the behavior of anisotropy in the central energy region.

Acknowledgments

The authors would like to thank Dr. S. Sugiyama for fruitful discussions and advice.

[1] J.G. Cordey and M.J. Houghton, Nucl. Fusion **13**, 215 (1973).
[2] T.H. Stix, Nucl. Fusion **15**, 737 (1975).
[3] M. Yamagiwa, T. Takizuka and Y. Kishimoto, Nucl. Fusion **27**, 1773 (1987).
[4] M. Nocente, G. Gorini, J. Källne and M. Tardocchi, Nucl. Fusion **51**, 063011 (2011).
[5] Ya.I. Kolesnichenko, Nucl. Fusion **20**, 727 (1980).
[6] H. Matsuura and Y. Nakao, Phys. Plasmas **13**, 062507 (2006).
[7] H. Matsuura and Y. Nakao, Phys. Plasmas **16**, 042507 (2009).
[8] L. Ballabio, G. Gorini and J. Källne, Phys. Rev. E **55**, 3358 (1997).
[9] J. Källne *et al*., Phys. Rev. Let. **85**, 1246 (2000).
[10] C. Hellesen *et al*., Nucl. Fusion **50**, 022001 (2010).
[11] C. Hellesen *et al*., Rev. Sci. Instrum. **85**, 11D825 (2014).
[12] H. Matsuura and Y. Nakao, J. Plasma Fusion Res. SERIES **9**, 48 (2010).
[13] M. Drosg and O. Schwerer, Production of monoenergetic neutrons between 0.1 and 23 MeV: neutron energies and cross-sections, Handbook of Nuclear Activation Data (Vienna: IAEA) STI/DOC/10/273, ISBN 92-0-135087-2 (1987).
[14] T. Nishitani *et al*., IEEE Trans. Plasma Sci. **47**, 12 (2018).
[15] S. Sugiyama *et al*., Nucl. Fusion **60**, 076017 (2020).
[16] H. Matsuura *et al*., IEEE Trans. Plasma Sci. **46**, 2301 (2018).
[17] S. Sugiyama *et al*., Phys. Plasmas **24**, 092517 (2017).
[18] J. Källne, P. Batistoni and G. Gorini, Rev. Sci. Instrum. **62**, 2781 (1991).
[19] G. Ericsson *et al*., Rev. Sci. Instrum. **81**, 10D324 (2010).
[20] J. Källne *et al*., Rev. Sci. Instrum. **68**, 581 (1997).
[21] K. Okada *et al*., 32nd EPS Conference on Plasma Phys. Tarragona, 27 June - 1 July 2005 ECA Vol.**29C**, P-4.096 (2005).
[22] Y. Kawamoto and H. Matsuura, J. Plasma Fusion Res. **11**, 2405078 (2016).
[23] J.D. Gaffey, Jr., J. Plasma Phys. **16**, 149 (1976).
[24] H. Brysk, Plasma Phys. **15**, 611 (1973).
[25] M.E. Swan *et al*., Proceedings of the 22nd IEEE / NPSSS symposium on Fusion Engineering, Albuquerque, HM. June 17-21, 1 (2007).
[26] Y. Nagaya, K. Okumura, T. Mori and M. Nakagawa, JAERI 1348 (2005).
[27] K. Shibata *et al*., J. Nucl. Sci. Technol. **48**, 1 (2011).